Morphological and Structural Features of Activated Iron Silicalites: A ^{129}Xe-NMR and EPR Investigation

Silvia Faggian,[†] Paola Fisicaro,[†] Elio Giamello,*[,†,§] Roberto Gobetto,[†] Alessandra Viale,[†] Gloria Berlier,[†] Carlo Lamberti,[†,§] and Ilenia Rossetti[‡]

Dipartimento di Chimica IFM, Università di Torino, Via P. Giuria 7, 10125 Torino, Italy, Dipartimento di Chimica Fisica ed Elettrochimica, Università di Milano, via C. Golgi 19, 20133 Milano, Italy, and INFM UdR di Torino Università, 10125 Torino, Italy

Received: September 26, 2002; In Final Form: April 4, 2003

^{129}Xe-NMR has been employed in the characterization of the activation of two iron silicalites, with different iron loadings. The ^{129}Xe chemical shift recorded as a function of the gas pressure is extremely sensitive to the state of the system and in particular to the hydration and oxidation state of extraframework iron ions. The NMR spectrum is composed of two main lines. The first one (in the range 120−140 ppm) is due to the interaction with the silicalite walls of the channels, while the second one (120−220 ppm) is due to the interaction with iron ions. The intensity and the chemical shift values of this peak markedly depend on the amount of iron in the system and, in particular, on the amount of iron ions dislodged from the framework and on the oxidation state. Thermal activation brings about a progressive dislodgment of iron ions from the framework positions and their partial reduction to Fe(II). Upon activation at 973 K, particularly large oxo−iron moieties are formed that (at least in the case of the higher loaded sample) prevent penetration of Xe atoms in the silicalite channels. The steric hindrance is removed both by further reduction in hydrogen and rehydration of the sample. The description of this complex phenomenology has been possible by comparing ^{129}Xe-NMR data with EPR data (which directly monitor the oxidation state of the systems and the effect of hydration−dehydration) and by performing parallel experiments on an Fe-exchanged ZSM-5 zeolite containing exclusively extraframework iron. The ^{129}Xe-NMR technique proved to be an excellent tool to characterize the systems and, potentially, other iron-containing porous materials.

Introduction

A great deal of activity in the field of heterogeneous catalysis has recently been devoted to MFI zeolitic systems containing trivalent iron in framework positions (iron silicalites).[1−4] It has been shown that these systems are active in the direct one-step oxidation of benzene to phenol using nitrous oxide as an oxidizing agent.[5,6] Iron silicalite, however, becomes catalytically active only after an activation process at high temperature, during which a fraction of the tetrahedral isolated iron ions is dislodged from the framework and is stabilized in various forms within the channels of the zeolite. The presence of extraframework iron brings about the onset of previously absent redox properties which, together with the acid properties of the system, are thought to be responsible for the catalytic activity. In particular, extraframework iron species are responsible for the formation of the so-called "α-oxygen" species, formed by adsorption of N_2O, that are responsible for the direct oxidation of benzene,[5,7] whose true nature has not yet been unambiguously explained.

Knowledge of the morphological and structural features of the catalyst after thermal activation is a key step in understanding its catalytic behavior. For this reason the characterization of the highly complex active catalyst is the target of intense research activity based on the simultaneous use of a variety of complementary experimental techniques.[8−16] Open questions are (i) the nature of the different extraframework sites formed during treatment, with particular attention to isolated and clustered species; (ii) the redox properties of extraframework iron ions; and (iii) the size of the clustered iron species present in the zeolite channels and the influence of iron loading and thermal treatments on this parameter.

A broad investigation of the properties of iron silicalites based on infrared spectroscopy, XANES, EPR, and on the systematic use of various molecules to probe the active sites of the system has been recently published by some of us;[15] it allowed us to become aware of the remarkably high complexity of the extraframework iron system and to attempt a first, not yet accomplished, picture of the various iron species present.

In the present paper we report an investigation of iron silicalite based essentially on the NMR of adsorbed xenon-129.[17,18] We chose this technique with the aim of using a probe with a (hypothetical) great potential for morphological description of the system. The size of the Xe atom (about 4.4 Å in diameter) is just slightly smaller than the size of the typical MFI channels (about 5.5 Å) so that the penetration and diffusion of this gas into the channels could be severely limited by the formation of clustered iron particles. The NMR results will be compared with those obtained by EPR of Fe^{3+} on the same samples under the same experimental conditions. EPR is not used here to obtain novel information on the spectroscopic features (e.g., spin-Hamiltonian parameters) of intrazeolitic ferric ions but, rather, to gather information on the general state of iron (aggregation, oxidation state) to better understand the ^{129}Xe-NMR results.

To clarify the role of extraframework iron ions in the system, we have also performed some experiments on ZSM-5 samples where iron ions were inserted by exchange from solution and are thus all located in extraframework positions. As will be

* Corresponding author. Phone: +39-011-6707574. Fax: +39-011-6707855. E-mail: elio.giamello@unito.it.
[†] Dipartimento di Chimica IFM, Università di Torino.
[‡] Dipartimento di Chimica Fisica ed Elettrochimica, Università di Milano.
[§] NFM UdR di Torino Università.

10.1021/jp027074c CCC: $25.00
Published on Web 07/29/2003

shown in the following, the ^{129}Xe-NMR technique (which, to our knowledge, has never been previously used to investigate iron-containing MFI zeolites), coupled with EPR spectroscopy, proved to be extremely sensitive to monitor the state of the catalyst after the various treatments.

Experimental

Two types of systems have been investigated in the present work. The first type of sample, prepared by the hydrothermal method, contains iron in isomorphous substitution and can be an iron silicalite (hereafter Fe-SIL), or an iron ZSM-5 (Fe-ZSM-5) when Al^{3+} is also present in the framework. In the second type of sample, iron has been introduced into H/ZSM-5 by ion-exchange from aqueous solutions. These samples will be hereafter indicated as Fe^{ex}/ZSM-5. The iron content (wt %) of each sample is indicated as a subscript of the symbol Fe. Two different iron silicalites, characterized by an Fe percentage of 1.40% and 0.35% ($Fe_{1.40}$-SIL and $Fe_{0.35}$-SIL, respectively) have been investigated together with one $Fe_{0.07}$-ZSM-5 and one $Fe^{ex}_{0.07}$/ZSM-5 system. The Al_2O_3 content of ZSM-5 systems was 4.28 and 0.98 wt %, respectively.

Fe-SIL and $Fe_{0.07}$-ZSM-5 have been synthesized by a hydrothermal method, as illustrated in ref 19, using tetrapropylammonium hydroxide as the templating agent, and adding the proper amount of $Fe(NO_3)_3$ to the gel. In this way, iron ions enter the MFI lattice during synthesis. The samples were washed with water and dried in air at room temperature. To eliminate the template, all the silicalite and zeolite samples were calcined first in dynamic vacuum at 773 K for 12 h with a temperature gradient of 3 K/min, then in oxygen atmosphere at 773 K for 5 h. To perform the described operation, 3 g of the powder was placed in the bottom of a wide quartz tube (diameter 2 cm) which was placed in the furnace. In such conditions (shallow bed) the treated material is expected to be homogeneous.

The $Fe^{ex}_{0.07}$/ZSM-5 sample was prepared by ion-exchange in aqueous solution as follows: 2.0 g of H-ZSM-5 was stirred for 48 h under nitrogen atmosphere at room temperature in a 1.0 mM $FeSO_4$ solution, containing 4.0 mg of ascorbic acid, to prevent iron oxidation. The solid was then washed with distilled water and dried in air at room temperature.

^{129}Xe-NMR and EPR spectra have been recorded on samples activated in vacuo at different temperatures, and after different redox treatments. The ^{129}Xe chemical shift was measured (and is reported in the following) as a function of Xe pressure. Natural-abundance xenon, purchased from Rivoira S.p.A. (Chivasso, Italy), has been used for the NMR measurements.

EPR spectra have been recorded at 77 K (in order to obtain more intense signals) on a Bruker EMX spectrometer, operating in X-band.

The ^{129}Xe-NMR spectra have been recorded at room temperature on a JEOL EX-400 spectrometer, operating at 110.64 MHz. The number of scans varied from 100 to 2500, depending on the sample. The chemical shift of Xe gas extrapolated to zero Xe pressure was fixed at 0.00 ppm as the reference for all the spectra.

To record the NMR spectra, the silicalite/zeolite samples were placed inside a 5 mm NMR quartz tube having a volume of about 3 mL, equipped with a vacuum valve and an adapter for the connection to a vacuum line. The height of the powdered sample in the NMR tube occupied ca. 2 cm at the bottom of the tube. The treatments were made directly in the NMR tube connected to the vacuum line. Gaseous Xe was then introduced at room temperature, the valve was closed, and the tube was transferred into the magnet for measurements. The same tube was used for EPR experiments. The treatments under hydrogen or oxygen were carried out in the NMR tube, under the following experimental conditions: 150 Torr of gas at 773 K for 2 h, followed by degassing the sample at room temperature for 30 min. Rehydration was carried out by introducing 20 Torr of water vapor into the tube at room temperature.

Results and Discussion

1. Chemical Shift of ^{129}Xe in Porous Systems. As proposed by Fraissard and co-workers, the ^{129}Xe chemical shift for xenon adsorbed on surfaces is given by the following expression which takes into account all the possible interactions between a xenon atom and its environment:[17,18]

$$\delta = \delta_{ref} + \delta_{Xe} + \delta_S + \delta_{SAS} + \delta_M + \delta_E \qquad (1)$$

In eq 1, δ_{ref} is the reference (chemical shift of Xe gas at $p \rightarrow 0$). δ_{Xe} is due to Xe−Xe interactions and depends directly on the local density of Xe or, alternatively, depends inversely on the free volume of the pores. The term δ_S accounts for the Xe interaction with a uniform surface and depends only on the nature of the surface and on the strength of its interaction with Xe atoms. δ_{SAS} is the contribution arising when strong adsorption sites (SAS) are present on the surface. This term is predominant at low coverage, i.e., in conditions when Xe atoms preferentially interact with the stronger surface sites. While the first three terms in eq 1 give rise to a linear trend of δ as a function of Xe concentration, the trend becomes parabolic when SAS are present. The chemical shift extrapolated to zero Xe concentration depends, in this case, upon the number and type of the strong adsorption sites. In the presence of paramagnetic cations, the observed chemical shift is further increased due to the δ_E and δ_M contributions, which correspond to the effect of the electric field and the magnetic field (if any) induced by these ions.

From the measurements of the ^{129}Xe chemical shift and from the shape of the plots of δ vs Xe concentration, it is then possible to obtain useful information about the presence and the nature of the adsorption sites in the porous systems, along with information about their location inside the pores and the size of the cavities accessible to Xe.

In general, each type of adsorption site should correspond to a different ^{129}Xe signal, but this is only true when the diffusion of Xe inside the pores is slow on the NMR time scale; otherwise averaged signals are observed. The spectra in the latter case are less informative so that the temperature of the system is, in some cases, decreased to slow the rate of Xe diffusion.[17]

Several examples of ^{129}Xe-NMR studies on zeolites containing various types of diamagnetic and paramagnetic cations are available in the literature.[24−32] To the best of our knowledge, however, no examples of Fe-containing systems have been reported up to now. Furthermore, most of the papers about systems containing paramagnetic metal ions refer to X and Y zeolites,[24−28] while, for MFI systems, mainly the effect of the Si/Al ratio[29] has been investigated by ^{129}Xe-NMR spectroscopy.

2. Fe-SIL Samples Activated in Vacuo at Moderate Temperature (298−473 K). If a sample of Fe-SIL still containing the templating agent in the channels is exposed to Xe pressure, no ^{129}Xe signal is detected in the NMR spectrum, except that of Xe gas; in this sample Xe atoms cannot enter the pores of the silicalite, which are occupied by the template molecules, and the gas adsorbed on the external surface is not detectable probably because of fast exchange with free Xe. This implies that all the signals that are observed at $\delta \neq 0$ on the

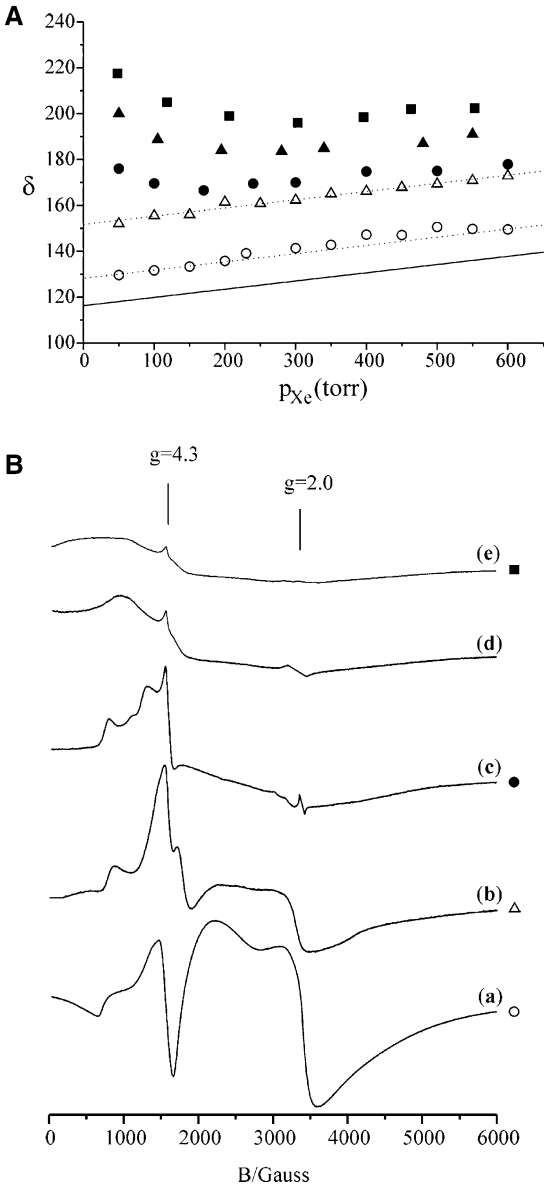

Figure 1. (A) δ vs p_{Xe} for a sample of $Fe_{1.40}$-SIL as a function of the sample treatment. SIL activated under vacuum at 298, 473, and 773 K (—); $Fe_{1.40}$-SIL activated under vacuum at 298 K (○) and 473 K (△), peak **A**; $Fe_{1.40}$-SIL activated under vacuum at 773 K, peak **B** (●); $Fe_{1.40}$-SIL reduced in hydrogen atmosphere after activation under vacuum at 773 K (▲) and 973 K (■), peak **B**. (B) EPR spectra, recorded at 77 K, of an $Fe_{1.40}$-SIL sample activated under vacuum at 298 K (a), at 473 K (b), at 773 K (c), at 973 K (d), and reduced in H_2 atmosphere at 773 K (e).

calcined sample (i.e., after the removal of the organic molecule from the channels) are due to Xe adsorbed *inside* the pores.

The plots of δ vs Xe pressure for $Fe_{1.40}$-SIL and $Fe_{0.35}$-SIL after calcination to eliminate the template and then outgassing at various temperatures are reported in Figure 1A and Figure 2, respectively. In both figures, the line corresponding to the interaction of Xe with a sample of bare, iron-free, silicalite (SIL, a MFI structure with SiO_2 stoichiometry) is reported (full line) as a reference. The same line was observed for samples of SIL outgassed at any temperature in the range 298−773 K.

When the two Fe-SIL samples are treated in vacuo in the 298−473 K range, only one NMR signal is observed with half-height width of about 1000 Hz (peak **A**, see Figure 3a, 3b): this signal is due to adsorbed ^{129}Xe and is analogous to that observed for the SIL samples. Its line width is about four times

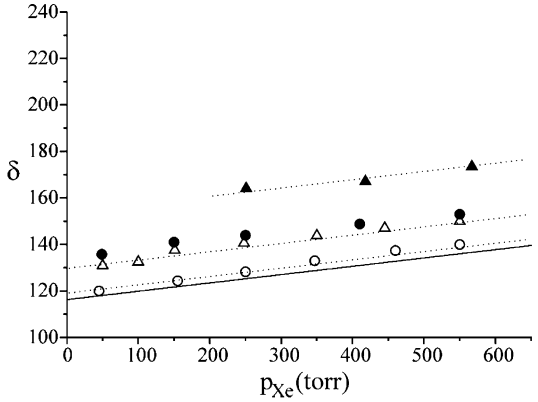

Figure 2. δ vs p_{Xe} for a sample of $Fe_{0.35}$-SIL as a function of the sample treatment. SIL activated under vacuum at 298, 473, and 773 K (—); $Fe_{0.35}$-SIL activated under vacuum at 298 K (○) and 473 K (△), peak **A**; $Fe_{0.35}$-SIL activated under vacuum at 773 K ≤ T ≤ 973 K, peak **B** (●); $Fe_{0.35}$-SIL reduced in hydrogen atmosphere after activation under vacuum at 973 K, peak **B** (▲).

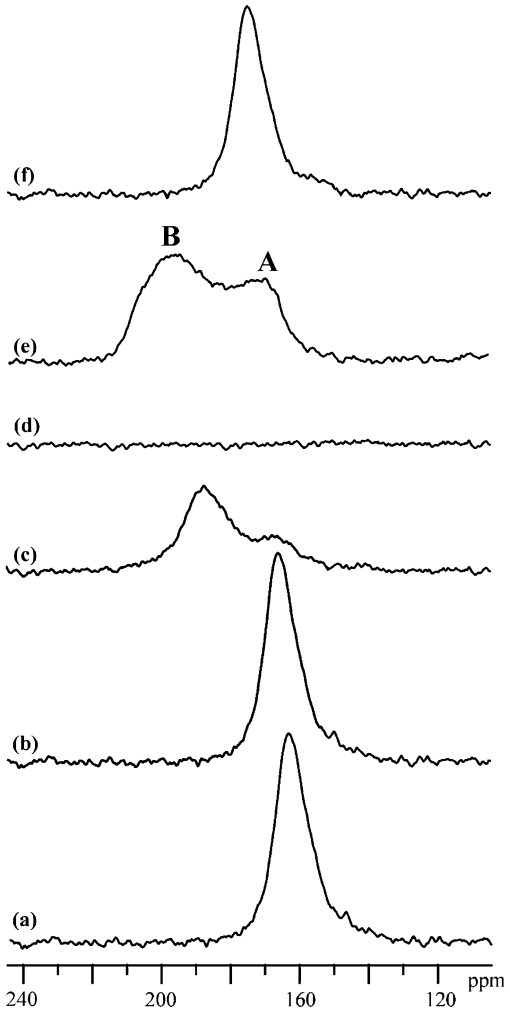

Figure 3. ^{129}Xe-NMR spectra (recorded 15 min after introduction of Xe, p_{Xe} = 600 Torr) of $Fe_{1.40}$-SIL activated under vacuum at 298 K (100 scans, a), 473 K (100 scans, b), 773 K (1000 scans, c), 973 K (2500 scans, d), 973 K and then reduced under hydrogen atmosphere (100 scans, e), 973 K and then rehydrated (100 scans, f).

larger than that observed for the corresponding signal of SIL samples, due to the presence of iron in the framework of Fe-SIL and, namely, to the relaxing effect of the paramagnetic Fe(III) ions. The plots of δ vs p_{Xe} for this signal are linear for both the Fe-SIL samples and show the same slope as the

corresponding line for SIL (see Figures 1A and 2, open symbols). A shift toward higher frequency with respect to SIL is, however, observed which is, again, due to the presence of framework Fe(III), which contributes to the chemical shift by the terms δ_M and δ_E in eq 1. As expected, the shift is larger for $Fe_{1.40}$-SIL due to the larger concentration of Fe(III) in the sample. Furthermore, the shift is larger for the two samples outgassed at 473 K than for those outgassed at 298 K.

To better understand the effects of thermal treatments on the state of the samples, the δ vs p_{Xe} plots of $Fe_{1.40}$-SIL are compared with the EPR spectra (Figure 1B) recorded under the same conditions. After outgassing at 298 K, the EPR spectrum (spectrum (a)) is dominated by a central broad line ($g \approx 2.00$) that can be assigned to ferric ions in a rather symmetric environment because of the coordination of water molecules on the framework iron ions.[14] Raising the outgassing temperature to 473 K reduces the amount of hydrated species (Figure 1B, spectrum (b)) with parallel increase of the amount of Fe^{3+} species in a distorted tetrahedral environment resonating at low magnetic field ($g \geq 4.3$). This explains the increase of the chemical shifts observed in Figure 1A passing from the samples outgassed at 298 K to those outgassed at 473 K. At higher temperature, the water molecules adsorbed on the silicalite channel surface tend to be removed and allow the Xe atoms to better approach the surface and the iron ions of the solid network.

3. EPR of Fe-SIL Samples Activated in Vacuo at High Temperature (773−973 K). When the samples are treated in a vacuum at 773 K $\leq T \leq$ 973 K, various phenomena are observed involving the intensity and the structure of both EPR and NMR lines. As far as EPR is concerned, when the temperature is raised to 773 K the central broad line at $g \approx 2.0$ practically vanishes while the lines at $g \geq 4.3$ (isolated iron species in distorted environment) reach their maximum intensity (Figure 1B, spectrum (c)). The whole spectral intensity, however, decreases after this treatment. The observed evolution is related to the progressive dehydration which leads to both EPR visible isolated species ($g \geq 4.3$) and also to some EPR silent ones, likely highly asymmetric species. No reduction of ferric ions occurs in this range of temperatures as the spectrum in Figure 1B(a) is fully recovered when rehydrating the sample in water vapor at room temperature. After outgassing at 973 K, the whole spectrum becomes very weak (Figure 1B, spectrum (d)) and the lines at low field ($g \geq 4.3$) become less structured. This is due both to the onset of the dislodgement of iron ions with formation of disordered structures in the channels (decrease of peaks at $g \geq 4.3$) and to the partial reduction of iron ions in Fe-SIL which starts for treatments at $T >$ 773 K.[14−15] The intensity decrease observed passing from spectrum (c) to spectrum (d) cannot be accounted for simply on the basis of highly asymmetric, EPR silent, Fe^{3+} coordination as for the experiments at $T <$ 773 K. This is shown by the fact that rehydration after outgassing at 973 K does not restore the initial situation. For this reason the onset of a partial reduction of iron to Fe^{2+} has to be taken into account, as also indicated by other experimental techniques.[15,16]

4. ^{129}Xe-NMR of Fe-SIL Samples Activated in Vacuo at High Temperature (773−973 K). A complex evolution of the structural and redox state of the system after high-temperature treatments is reflected also in the ^{129}Xe-NMR results. The most relevant facts observed by this technique are summarized in the following five points.

(i) A second broader resonance (**B**) appears at higher frequency beside peak **A** starting from 773 K (Figure 3(c)). The relative intensities of both peaks vary with time as shown in Figure 4. The initial intensity of peak **B** remains roughly constant while that of peak **A** increases, until an equilibrium is reached. This behavior is the same for both Fe-SIL samples, except for the fact that in the case of $Fe_{0.35}$-SIL the final intensity of peak **B** is lower than that of the corresponding peak in $Fe_{1.40}$-SIL, and its evolution with time is somewhat faster.

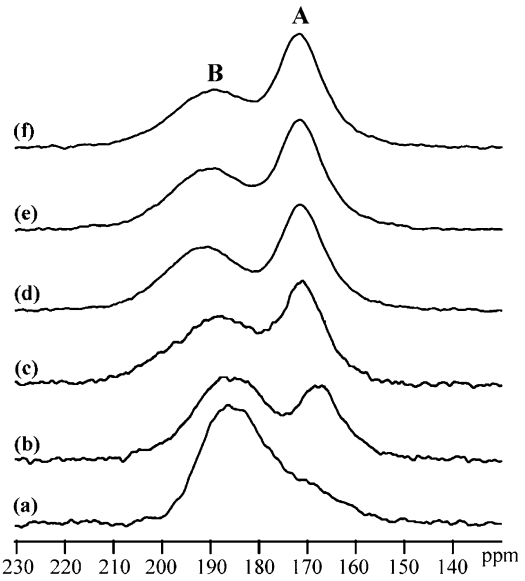

Figure 4. Evolution of peaks **A** and **B** with time for a sample of $Fe_{1.40}$-SIL activated under vacuum at 773 K: spectra recorded at RT after 5 (a), 20 (b), 40 (c), 55 (d), 70 (e), and 100 (f) min after the introduction of xenon into the tube (p_{Xe} = 600 Torr).

(ii) The chemical shift of signal **B** increases when increasing the activation temperature above 773 K. Simultaneously, however, the whole signal intensity decreases until the limiting situation observed at 973 K, when both **A** and **B** NMR lines are not observed in the case of the $Fe_{1.40}$-SIL sample (Figure 3(d)). However, the intensity remains at an acceptable level for the low-loading, $Fe_{0.35}$-SIL sample even after activation at 973 K (spectra not shown).

(iii) The reversibility of the EPR spectra upon rehydration (observed for samples outgassed up to 773 K) is reflected in the NMR spectra (line **B** disappears in rehydrated samples and the spectrum in Figure 3(a) is recovered).

(iv) Peaks **A** and **B** remain well separated even if the recording temperature of the NMR spectra is raised to 473 K. The only effect observed is an increase of the evolution rate of the two peaks toward equilibrium.

(v) While the trend of the chemical shift of peak **A** with pressure remains the same after activation at high temperature with respect to that observed at 473 K, that of peak **B** is treatment-dependent. The plots of the chemical shift of peak **B** vs p_{Xe} are reported in Figures 1A and 2 (curves with full symbols) for the two Fe-SIL samples, respectively.[1] (In all the figures reporting δ vs p_{Xe} plots (Figures 1, 2, 5), the data related to peaks of **A** and **B** type are indicated by open symbols and full symbols, respectively.) In the case of $Fe_{0.35}$-SIL the plot is still linear, while in that of $Fe_{1.40}$-SIL it shows a minimum for intermediate pressure values. This trend is typical of the presence of strong adsorption sites on the surface,[17,18] which contribute to δ by the term δ_{SAS} (eq 1).

The behavior summarized above is due to a multiplicity of complex phenomena which are presently under discussion in the literature. It is generally accepted[6,9,14−16] that during the activation steps from about 773 K, ferric ions start to migrate from the framework to the channels and undergo a rearrange-

ment of their environment. The appearance of peak **B** in the NMR spectra must thus be associated with the presence of dislodged iron ions in the channels. An interaction of these new moieties with Xe atoms is now possible and more intense than that possible for an iron embedded in the tetrahedral structure of unperturbed silicalite. This is reflected in the onset of the δ_{SAS} contribution to the chemical shift of peak **B**, evident from the trend of the δ vs p_{Xe} plot for $Fe_{1.40}$-SIL treated at 773 K (Figure 1A, ● parabolic shape). In the case of $Fe_{0.35}$-SIL treated at 773 K, the plot is still linear because the lower amount of Fe in the sample leads to a smaller concentration of strong adsorption sites after treatments at high temperature. Peak **B** (which is more intense and occurs at higher frequency in the sample containing more Fe ions) can then be confidently assigned to Xe adsorbed on extraframework Fe ions or small oxo−iron clusters located inside the channels. This agrees with (i) the higher chemical shift of peak **B** with respect to peak **A**, (ii) the onset of the contribution of the term δ_{SAS} to the chemical shift, particularly appreciable for a high Fe-loaded sample, and (iii) the wider line width of peak **B** with respect to **A**. In particular, the large line width of signal **B** may be due to the onset of a more efficient paramagnetic relaxation due to a lower distance between the Xe atom and the unpaired electrons of the iron ions, or, alternatively, to a substantial heterogeneity of the extraframework iron coordination.

To explain the appearance of peak **B** in samples outgassed at 773 K (whose situation has been described above as fully reversible to rehydration), it must be remembered here that all samples were submitted after preparation (and thus prior to any other thermal or chemical treatment) to the calcination at 773 K for template removal and that this treatment starts to modify and disorder the initial structure of all iron ions in framework positions.[14] The trend of the chemical shift observed after activation at 773 K may thus be due to some iron ions being dislodged in the channels by the initial calcination for template removal which can directly interact with xenon atoms only after the complete removal of OH^- groups.

The trend of the **A** and **B** band intensities with time, prior to equilibrium, reported in Figure 4 for the $Fe_{1.40}$-SIL sample treated at 773 K, can be explained as follows. The **B** band is only initially observed (4(a**)**) because of the higher sticking probability for Xe adsorption on the more energetic extraframework iron sites. The slow diffusion of the gas in the partially obstructed structure leads to the formation of peak **A** after 20 min. The relative intensity of **A** grows with time and, once the equilibrium is reached (Figure 4(f)), is clearly higher than that of **B**. The final intensity of **B**, however, is nearly the same as that observed in the early steps of the interaction, thus confirming the initial preferential interaction of Xe with the stronger sites available in the system.

A further comment is now devoted to the disappearance of both NMR lines in $Fe_{1.40}$-SIL treated at 973 K. This fact has to be related to the formation of extraframework clustered iron species whose size is large enough to limit the Xe diffusion into the channels. The diameter of the channels in MFI zeolites is about 5.5 Å, while the diameter of Xe atoms is about 4.4 Å. Even when a small aggregate is formed in the channel the diffusion of the gas inside the porous structure is considerably inhibited. This explains the progressive loss of intensity of the signals observed by raising the treatment temperature. This leads, for treatment at 973 K, to the total blockage of the Xe atom diffusion into the channels. The lower iron concentration in $Fe_{0.35}$-SIL and the consequent smaller amount and size of the extraframework particles that can be formed in this case are the reason that both **A** and **B** bands are always observed (even if with a lower signal-to-noise ratio) on this sample.

The total hindrance to Xe penetration can, however, be removed by rehydration of the system. After treating the sample outgassed at 973 K (Figure 3(d)) in water vapor at room temperature, the NMR spectrum in Figure 3(f) is observed which is constituted by the **A** line only. This finding suggests that hydration of the oxo−iron particles brings about a disruption process of these aggregates, in strict analogy to that observed for copper aggregates in ZSM-5 zeolites.[33] The presence in the spectrum of peak **A** only does not mean that the initial state of the sample is restored (EPR, vide supra, has definitely shown the irreversibility of the iron phase transformation beyond 773 K). It only suggests that hydroxyl groups or water molecules coordinating Fe ions after water adsorption act as a sort of screen between the iron ions and the Xe atoms, thus preventing the relatively strong interaction characterized by peak **B** which can be considered a probe of extraframework iron exclusively in fully dehydrated materials.

5. Fe-SIL Samples Reduced in Hydrogen. To better evidence the effects of Fe^{3+} reduction discussed in the previous section, the samples outgassed at high temperature (773 K, 973 K) were treated in reducing conditions, i.e., in H_2 atmosphere (100 Torr) at 773 K. After the reducing treatment, the EPR profile shown by both $Fe_{1.40}$-SIL and $Fe_{0.35}$-SIL is similar to that reported in Figure 1B (spectrum (e**)**) with, however, a remarkable decrease of the intensity. In these conditions the ferrous, Fe^{2+}, ions constitute the large majority of the iron in the system.

The reduction is accompanied by an interesting evolution of the NMR spectra which are summed up in the following.

(i) The sample reduced in H_2 after outgassing at 773 K still exhibits peaks **A** and **B**. The latter peak, however, now has higher chemical shift values and the resulting δ vs p_{Xe} curve (Figure 1A, line ▲) still exhibits a minimum like the sample simply outgassed at 773 K. This behavior indicates that the shift of peak **B** is induced by the reduction of the Fe(III) ions to Fe(II): the unpaired electron distribution around the nucleus is distorted in Fe(II) (a d^6 ion), with respect to Fe(III) (an S state, d^5 ion), thus leading to a larger paramagnetic shift. The chemical shift increase due to iron reduction is observed also in the case of the low-loading samples ($Fe_{0.35}$-SIL) upon treatment in H_2 (Figure 2, curve ▲).

(ii) The $Fe_{1.40}$-SIL sample outgassed at 973 K, and NMR-silent after this process (Figure 3(d**)**), becomes NMR-active after reduction, and both **A** and **B** peaks reappear. The profile of the δ vs p_{Xe} curve is reported in Figure 1A (line ■) and shows a further increase of the chemical shift values. This must be due to the largest amount of extraframework Fe(III) ions that are available for reduction after the strong activating treatment at 973 K. The surprising result of this experiment is, however, the fact that after reduction in H_2 the zeolite channels become again accessible to the Xe atoms. This should mean that the reduction process is accompanied by a disruption of those oxo−iron microaggregates which severely limits the gas diffusion into the structure.

In conclusion, the hindrance to the diffusion of gases into the channels is maximal for samples activated at high temperature (973 K) but decreases upon reduction or, as shown in the previous section, upon rehydration.

6. Ion-Exchanged $Fe^{ex}_{0.07}$/ZSM5. To confirm the hypothesis about the role of extraframework ions in the behavior of high-temperature-activated Fe-SIL samples, the NMR experiments performed on the latter ones were repeated for a low-loading

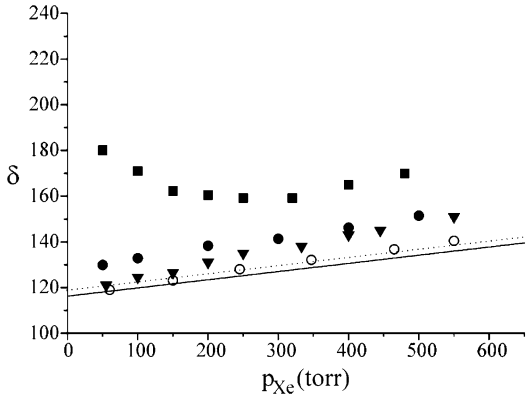

Figure 5. δ vs p_{Xe} for a sample of $Fe^{ex}_{0.07}$/ZSM-5 as a function of the sample treatment. H/ZSM-5 activated under vacuum at 298, 473, and 773 K (—); $Fe^{ex}_{0.07}$/ZSM5-activated under vacuum at 298 K, peak **A** (○); $Fe^{ex}_{0.07}$/ZSM-5 activated under vacuum at 473 K (▼), and at 773 K (■), peak **B**; $Fe^{ex}_{0.07}$/ZSM-5 activated under vacuum at 773 K and oxidized in oxygen atmosphere, peak **B** (●).

sample ($Fe^{ex}_{0.07}$/ZSM5) obtained by ion-exchange of a H-ZSM5 in a solution of Fe^{2+} ions. This sample therefore exclusively contains iron species in the channels.

The use of a ZSM5 matrix (containing Al^{3+} in the framework) for preparing an exchanged material is unavoidable in that no exchange can be performed with a pure silicalite. However, the possible influence of framework Al^{3+} on the ^{129}Xe chemical shift was checked in advance on a H-ZSM5 sample at various degrees of dehydration, and no difference was observed between these values and those recorded for a bare silicalite (SIL).

The results recorded after submitting the exchanged sample containing Fe(II) to the same treatments adopted for iron silicalites are collected in Figure 5. The trend of the δ vs pressure plots is basically the same found in the previous cases, but some considerations are now needed.

(i) Peaks **A** and **B** are in this case well separated, indicating a slow Xe diffusion inside the channels.

(ii) Peak **B** (Xe on extraframework Fe species) appears in the spectra after activation at 473 K (i.e., at a temperature 300 K lower than that needed for $Fe_{0.07}$-ZSM-5 to observe the same phenomenon) and its intensity in the case of $Fe^{ex}_{0.07}$/ZSM5 is quite high compared with that observed for $Fe_{0.07}$-ZSM-5 (a ZSM system with framework iron) activated at 773 K. Furthermore, by comparing the chemical shift values of these two samples at the same activation temperature and Xe pressure, one may notice that the chemical shift of peak **B** for $Fe_{0.07}$-ZSM-5 is about 40 ppm lower than that of $Fe^{ex}_{0.07}$/ZSM-5. This fact, together with the appearance of peak **B** at relatively low activation temperature (473 K), indicates, as expected, the presence in the exchanged zeolite of a larger concentration of strong adsorption sites (the Fe ions) inside the channels. These strong adsorption sites are also responsible for the curvature of the plot of δ vs p_{Xe} (Figure 5, ■). A further contribution (maybe the most important) to the observed increase in the chemical shift comes from the reductive process of the Fe(III) present in the sample occurring during the activation of $Fe^{ex}_{0.07}$/ZSM-5. EPR spectra, not reported here for the sake of brevity, confirm the easier reducibility of the exchanged sample in comparison to the Fe-SIL samples. The role of reduction to Fe(II) during activation is confirmed by the fact that the original chemical shift is recovered after reoxidation in an oxygen atmosphere (curve ● in Figure 5). The chemical shift of the oxidized sample shows a linear dependence upon Xe pressure, since in the oxidized form the iron entities are not sufficiently in contact with Xe atoms.

Conclusions

The joint use of EPR and ^{129}Xe-NMR spectroscopies and the comparison between samples containing framework iron species with samples submitted to ion-exchange from solutions (and thus exclusively containing extraframework species) has allowed a convincing description of the processes associated with the thermal activation of iron silicalite. In particular ^{129}Xe-NMR can be considered an excellent tool for monitoring the state of iron species in pentasilic zeolites: this is, in part, due to the critical dimension of the Xe atoms, which are about 1 Å smaller than the channel diameter of the system.

Two independent NMR lines have been detected:

(a) The **A** line (in the range 120−140 ppm) which is due to nonspecific interaction with the internal wall of the channels.

(b) The **B** line, which, according to the iron loading, is in the range from 120 and 220 ppm and is strictly correlated with the interaction of Xe with iron species. Its features (intensity, line width, chemical shift) depend on (i) the iron loading of the system, (ii) the amount of iron in the channels (the dislodgment of iron from the framework upon activation is monitored by a progressive increase of the **B** chemical shift), (iii) the oxidation state of iron (the **B** shift is higher for ferrous species ($3d^6$) than for ferric species ($3d^5$)), and (iv) the solvation degree of the iron ions (a full coordination sphere of water molecules reduces the magnetic contact between Xe and Fe ions).

In the present paper it has also been shown that the size of the extraframework iron complexes can grow to such a value that the diffusion of Xe in the channels is completely inhibited. Interestingly, upon reduction as well as rehydration, the size of these iron aggregates becomes smaller than the critical limit that blocks the Xe diffusion. The removal of the steric hindrance to Xe diffusion caused by the chemical transformation of the large oxidized oxo−iron aggregates is unambiguously monitored by the reappearance of the ^{129}Xe-NMR lines.

Acknowledgment. We thank Prof. Adriano Zecchina (Università di Torino) and Prof. Lucio Forni (Università di Milano) for helpful discussions. The financial aid of the Italian Ministry of University and Scientific and Technological Research (MURST), through the COFIN 1998-2000 program, is gratefully acknowledged.

References and Notes

(1) Szostak, R.; Thomas, T. L. *J. Catal.* **1986**, *100*, 555.
(2) Jacobs, P. A.; Beyer, H. K. *J. Phys. Chem.* **1979**, *83*, 1174.
(3) Feng, X.; Hall, W. K. *J. Catal.* **1997**, *166*, 368.
(4) Marturano, P.; Kogelbauer, A.; Prins, P. *J. Catal.* **2000**, *190*, 460.
(5) Gubelmann, M.; Tirel, P.-J. Fr. Patent 2,630,735, 1988.
(6) Kharitonov, A. S.; Alexandrova, T. N. L.; Vostrikova, A.; Ione, K. G.; Panov, G. I. Russ. Patent 4,445,646, 1988.
(7) Pirutko, L. V.; Chernyarsky, V. S.; Uriarte, A. K.; Panov, G. I. *Appl. Catal. A General* **2000**, *227*, 143.
(8) Marturano, P.; Drodzovà, L.; Kogelbauer, A.; Prins, P. *J. Catal.* **2000**, *192*, 236.
(9) Axon, S. A.; Fox, K. K.; Carr, S. W.; Klinowski, J. *Chem. Phys. Lett.* **1992**, *189*, 1.
(10) Lewis, D. W.; Catlow, R. A.; Sankar, J.; Carr, S. W. *J. Phys. Chem.* **1995**, *99*, 2377.
(11) El-Malki, El-M.; van Santen, R. A.; Sachtler, W. M. H. *J. Catal.* **2000**, *196*, 212.
(12) Chen, H. Y.; El-Malki, El-M.; Wang, X.; van Santen, R. A.; Sachtler, W. M. H. *J. Mol. Catal. A* **2000**, *162*, 160.
(13) Aparicio, L. M.; Hall, W. K.; Fang, S. M.; Ulla, M. A.; Millman, W. S.; Dumesic, J. A. *J. Catal.* **1987**, *108*, 233.
(14) Bordiga, S.; Buzzoni, R.; Geobaldo, F.; Lamberti, C.; Giamello, E.; Zecchina, A.; Leofanti, G.; Petrini, G.; Tozzola, G.; Vlaic, G. *J. Catal.* **1996**, *158*, 486.
(15) Berlier, G.; Spoto, G.; Bordiga, S.; Ricchiardi, G.; Fisicaro, P.; Zecchina, A.; Rossetti, I.; Selli, E.; Forni, L.; Giamello, E.; Lamberti, C. *J. Catal.* **2002**, *208*, 64.

(16) Berlier, G.; Spoto, G.; Fisicaro, P.; Bordiga, S.; Zecchina, A.; Giamello, E.; Lamberti, C. *Microchem J.* **2002**, *71*, 101.

(17) Springuel-Huet, M. A.; Bonardet, J. L.; Gedeon, A.; Fraissard, *J. Magn. Reson. Chem.* **1999**, *37*, S1 and references therein.

(18) Bonardet, J. L.; Fraissard, J.; Gedeon, A.; Springuel-Huet, M.-A. *Catal. Rev.*−*Sci. Eng.* **1999**, *41* (2), 115 and references therein.

(19) Ratnasamy, P.; Kumar, R. *Catal. Today* **1991**, *9*, 329.

(20) Goldfarb, D.; Bernardo, M.; Strohmaier, K. G.; Vaughan, D. E. W.; Thomann, H. *J. Am. Chem. Soc.* **1994**, *117*, 6344.

(21) Ferretti, A. M.; Forni, L.; Oliva, C.; Ponti, A. *Res. Chem. Intermed.* **2002**, *28*, 101.

(22) Feng, X.; Hall, W. K. *J. Catal*. **1997**, *166*, 368.

(23) Liu, S. B.; Fung, B. M.; Yang, T. C.; Hong, E. C.; Chang, C. T.; Shih, P. C.; Tong, F. H.; Chen, T. L. *J. Phys. Chem.* **1994**, *98*, 4393.

(24) Bansal, N.; Dybowski, C. *J. Phys. Chem.* **1988**, *92*, 2333.

(25) Gedeon, A.; Bonardet, J. L.; Ito, T.; Fraissard, J. *J. Phys. Chem.* **1989**, *93*, 2563.

(26) Liu, S. B.; Lin, T. S.; Yang, T. C.; Chen, T. H.; Hong, E. C.; Ryoo, R. *J. Phys. Chem*. **1995**, *99*, 8277;

(27) Shoemaker, R.; Apple, T. *J. Phys. Chem*. **1987**, *91*, 4024.

(28) Shy, D. S.; Chen, S. H.; Lievens, J.; Liu, S. B.; Chao, K. J. *J. Chem. Soc., Faraday Trans*. **1991**, *87*, 2855.

(29) de Menorval, L. C.; Fraissard, J.; Ito, T. *J. Chem. Soc., Faraday Trans*. **1982**, *78*, 403.

(30) Grosse, R.; Burmseister, R.; Boddenberg, B.; Gedeon, A.; Fraissard, J. *J. Phys. Chem.* **1991**, *95*, 2443.

(31) Cho, S. J.; Ahn, W. S.; Hong, S. B.; Ryoo, R. *J. Phys. Chem*. **1996**, *100*, 4996.

(32) Chen, Q.; Springuel-Huet, M. A.; Fraissard, J.; Smith, M. L.; Corbin, D. R.; Dybowski, C. *J. Phys. Chem*. **1992**, *96*, 10914.

(33) Turnes Palomino, G.; Fisicaro, P.; Bordiga, S.; Zecchina, A.; Giamello, E.; Lamberti, C. *J. Phys. Chem.* **2000**, *104*, 4064.